

# Aircraft profiles of aerosol microphysics and optical properties over North America: Aerosol optical depth and its association with PM2.5 and water uptake

Yohei Shinozuka,<sup>1</sup> Antony D. Clarke,<sup>1</sup> Steven G. Howell,<sup>1</sup> Vladimir N. Kapustin,<sup>1</sup> Cameron S. McNaughton,<sup>1</sup> Jingchuan Zhou,<sup>1</sup> and Bruce E. Anderson<sup>2</sup>

Received 13 August 2006; revised 18 February 2007; accepted 1 May 2007; published 21 June 2007.

[1] Aerosol column optical depth (AOD) is related to the aerosol direct radiative effect and readily available as a satellite product. The mass of dry aerosol up to 2.5  $\mu\text{m}$  aerodynamic, or PM2.5, is a common measure of surface aerosol pollution at selected regional sites. A link between these two parameters would provide a way to infer PM2.5 and its change over extensive regions observed by satellites. This requires determination of the response of aerosol dry mass to the widely variable influence of ambient humidity and its optical contribution to column AOD. During the INTEX-North America aircraft campaign, we obtained 72 profiles of visible aerosol light scattering up to 10 km and its response to water uptake. The ambient AODs determined from these measurements, and confirmed for three profiles near surface AERONET, were generally below 0.4 except in the presence of a humid boundary layer with high aerosol loading. The fraction of ambient AOD due to water uptake,  $W_f$ , was found to be  $37 \pm 15\%$  (average and standard deviation). Boundary layer PM2.5 was estimated (PM2.5<sub>proxy</sub>) from low-altitude size distributions measured from the aircraft. Despite the large variety of vertical aerosol structure, the ambient AOD was found correlated with the PM2.5<sub>proxy</sub> with  $R^2 = 0.77$ , after 4% of data with AOD > 0.8 for >90% RH were removed. Our results support the application of remote sensing to retrievals of surface PM2.5 mass. The wavelength dependence of ambient AOD was found to be less effective in stratifying the mass versus extinction relationship on the column integral basis than on a layer by layer basis.

**Citation:** Shinozuka, Y., A. D. Clarke, S. G. Howell, V. N. Kapustin, C. S. McNaughton, J. Zhou, and B. E. Anderson (2007), Aircraft profiles of aerosol microphysics and optical properties over North America: Aerosol optical depth and its association with PM2.5 and water uptake, *J. Geophys. Res.*, 112, D12S20, doi:10.1029/2006JD007918.

## 1. Introduction

[2] Aerosols affect Earth's radiative balance, hydrological and biogeochemical cycles, visibility and human health. Emissions, whether from urban/industrial sources such as cars and factories or from natural sources such as forest fires, desert and ocean surface, are typically reported as mass under dry conditions. The mass of aerosols up to an aerodynamic diameter of 2.5  $\mu\text{m}$ , or PM2.5, is widely monitored on ground (e.g., AIRNow, a U.S. government agency, <http://www.airnow.gov/>) and used to assess and regulate pollution.

[3] Aerosol optical depth (AOD) is a measure of the extinction of light passing throughout the atmosphere and is relevant to the direct radiative effect. Unlike PM2.5, AOD is

defined over the entire air column and readily available from radiance measurements with satellite and ground sensors at multiple wavelengths [Chu *et al.*, 1998; Holben *et al.*, 1998; Kahn *et al.*, 1998; Tanre *et al.*, 1997].

[4] If surface PM2.5 measurements are shown to relate strongly to radiance or AOD, there is potential for using satellites to infer PM2.5 with high resolution over regions not monitored with ground PM2.5 networks. Liu *et al.* [2004] and Liu *et al.* [2005] parameterized surface PM2.5 using satellite and model products and achieved moderate correlations with surface measurements on a seasonal average (not concurrent measurement) basis. Dubovik and King [2000] and Kaufman *et al.* [1997] translate radiance and its wavelength dependence measured with Sun photometers and the Moderate Resolution Imaging Spectroradiometer (MODIS) satellite into aerosol size distribution. Gassó and Hegg [2003] link the satellite products to column-integral (not near-surface) aerosol mass, and compared with measurements made with sizing instruments aboard aircraft. While various closure experiments in the past decade focused on validating surface AOD versus satellite AOD measurements [Chu *et al.*, 2002, 2003; Ichoku *et al.*, 2003; Remer *et al.*,

<sup>1</sup>School of Ocean and Earth Science and Technology, University of Hawaii, Honolulu, Hawaii, USA.

<sup>2</sup>Atmospheric Sciences Division, NASA Langley Research Center, Hampton, Virginia, USA.

2002], limited in situ data is available for comparison of surface PM<sub>2.5</sub> with satellite radiances [Wang and Christopher, 2003].

[5] In translating remotely sensed column optical properties into dry aerosol mass, relative humidity (RH) needs to be considered. Hygroscopic aerosol components respond to increasing RH by growing in size and scattering more light [Howell *et al.*, 2006; Malm *et al.*, 1994; Tang and Munkelwitz, 1991]. Both aerosol models and remote sensing attempt to account for these humidification effects though using different input variables and methods. In situ observations can provide means to identify how well models compute ambient AOD given dry aerosol size distributions, water uptake and ambient RH and, as demonstrated by Gassó and Hegg [2003], how accurately remotely sensed ambient AOD can be translated into dry AOD and mass.

[6] The goal of this paper is to examine AOD response to water uptake and its relationship to PM<sub>2.5</sub> by taking advantage of aircraft profiles over extensive regions of North America. The AOD is calculated at the ambient RH conditions for 72 profiles made during descents and ascents, using scattering coefficients measured under both low and near-ambient RH. Results are compared with independent ground measurements when possible. A PM<sub>2.5</sub><sub>proxy</sub> for dry aerosols is calculated from size distributions measured at  $500 \pm 200$  m. To stratify the resulting AOD versus PM<sub>2.5</sub><sub>proxy</sub> relationship, we also calculate the relative contributions from different altitudes and those from the aqueous component to the AOD.

## 2. Measurements and Instrumentation

[7] We collected data during the Intercontinental Chemical Transport Experiment-North America (INTEX-NA) experiment, a major NASA science campaign to understand the transport and transformation of gases and aerosols on transcontinental and intercontinental scales and their impact on air quality and climate. The NASA DC-8 research aircraft was deployed mostly over the eastern half of the continental United States and the Atlantic Ocean off the U.S. east coast from 1 July to 15 August 2004 as described by Singh *et al.* [2006].

[8] Aerosols were conveyed to the aerosol instrumentation aboard the DC-8 aircraft using the University of Hawaii solid diffuser inlet. This inlet and sample plumbing has recently been shown to pass aerosol with dry aerodynamic diameter of  $4.8 \mu\text{m}$  with better than 50% efficiency [McNaughton *et al.*, 2007].

[9] Total and submicrometer aerosol scattering coefficients were measured using two TSI model 3563 three-wavelength integrating nephelometers [Anderson *et al.*, 1996; Heintzenberg and Charlson, 1996]. The submicrometer TSI nephelometer employed a  $1\text{-}\mu\text{m}$  aerodynamic impactor maintained at 30 lpm by an Alicat Scientific volumetric flow controller. Sample air residence time inside the nephelometers was about 10 s, and the instrument relative humidity (RH) usually lower than 30%.

[10] Two single-wavelength (near 540 nm) Radiance Research model M903 nephelometers were operated in parallel, one at 80% (RH<sub>1</sub>) and the other at <40% (RH<sub>2</sub>) to provide RH sensitivity of aerosol scattering [Howell *et*

*al.*, 2006]. The wet to dry scattering ratio,  $f(\text{RH})$ , was averaged for 60 s and used to calculate  $\gamma$  on the basis of equation (1).

$$f(\text{RH}) = ((1 - \text{RH}_1/100)/(1 - \text{RH}_2/100))^{-\gamma} \quad (1)$$

$\gamma$  characterizes scattering response that is determined by the aerosol chemistry, mixing state, sizes and refractive index. These are primarily determined by source type and location as well as transport and scavenging processes, and not directly related to ambient RH. Using the calculated  $\gamma$ , we can calculate  $f(\text{RH})$  for the ambient RH, or  $f(\text{ambRH})$ , by replacing RH<sub>1</sub> and RH<sub>2</sub> with the measured ambient RH and the TSI nephelometer (<40%) RH, respectively. The resulting  $f(\text{ambRH})$ , when multiplied to the total dry scattering coefficient measured with the TSI nephelometer at 550 nm, gives the scattering coefficient under the ambient RH.

[11] A prototype three-wavelength Radiance Research particle soot absorption photometer was provided by Dr. David Covert (University of Washington) to measure aerosol light absorption at 470, 530, 660 nm. The absorption coefficients are based upon calibration for this new instrument reported elsewhere [Virkkula *et al.*, 2005], but some recent indications suggest result may differ from the true absorption by about 20%. In the present study the absorption at 530 nm is used to relate the scattering coefficient to extinction. Because the absorption rarely exceeded 10% of extinction integrated over vertical profiles, the measurement uncertainty results in a 2% or less error in estimated aerosol optical depth.

[12] An optical particle counter (OPC, a modified LAS-X, Particle Measurement Systems, Boulder, Colorado) measured the dry (RH < 30%) aerosol size distribution between  $0.1 \mu\text{m}$  and about  $10 \mu\text{m}$  [Clarke, 1991]. The particle size was calibrated with polystyrene latex spheres whose refractive index is 1.59. The data was obtained every 3 s, but averaged over 30–60 s to reduce error due to low counting statistics at about  $1 \mu\text{m}$  or larger. The He-Ne laser operates at 633 nm detecting light scattered by individual particles over  $35\text{--}145^\circ$ . Since the OPC measures optically, it is well suited to modeling aerosol optical properties.

## 3. OPC Validation

[13] In this study the dry size distribution measured with the OPC is used to model the ambient response of scattering to water uptake as well as to estimate the dry aerosol mass. It is evaluated here against the concurrent dry nephelometer measurements. The uncertainty in the derived volume is also considered.

[14] Scattering coefficient at 550 nm was calculated using Mie theory from the OPC distribution for the TSI nephelometer detection angle ( $7\text{--}170^\circ$ ). For comparison with the submicron scattering coefficient, we used the size distribution up to  $0.75 \mu\text{m}$  [McMurry *et al.*, 2002]. Figure 1 shows 30–45 s averages of derived scattering coefficients for all horizontal flight legs during INTEX-NA. The calculated scattering coefficients over both size ranges are within 10% of the measured scattering values with correlation coefficients of 0.95. The submicron agreement is better than the total that suffers poorer coarse particle counting statistics.

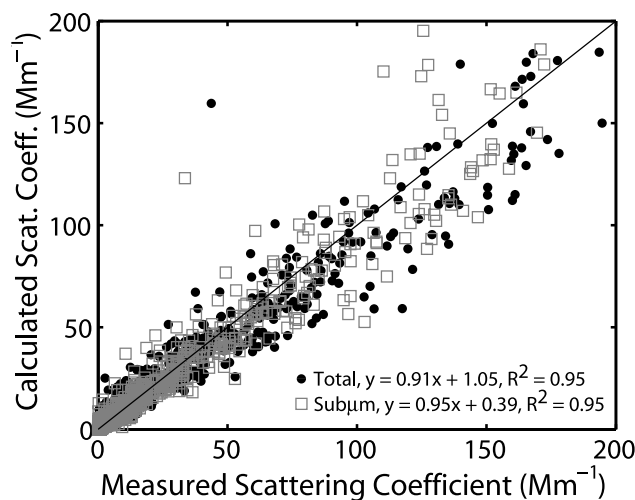


**Figure 1.** Scattering coefficient derived from the OPC size distribution compared to the nephelometer direct measurement under dry conditions. The particle size ranges are 0.1–20  $\mu\text{m}$  (dot) and 0.1–1  $\mu\text{m}$  (square).

The intercept of 0.39  $\text{Mm}^{-1}$  is reasonable, because it is comparable to TSI nephelometer noise level for a 30-s average ( $\sim 0.3 \text{ Mm}^{-1}$ ) [Anderson *et al.*, 1996]. Uncertainties in sample flow rate ( $\sim 3\%$ ) and refractive index may contribute to the nonideality too.

[15] OPC particle sizing is sensitive to the refractive index,  $n$ , of the sampled particles [Pinnick *et al.*, 2000]. Silica test particles ( $n = 1.45\text{--}1.46$ ) with diameters 0.73  $\mu\text{m}$  and 1.58  $\mu\text{m}$  appear at sizes 0.63  $\mu\text{m}$  and 1.25  $\mu\text{m}$ , respectively for the PSL-calibrated ( $n = 1.59$ ) OPC, showing similar degrees of sensitivity to that demonstrated in a previous study with oleic acid ( $n = 1.46$ ) particles [Hand and Kreidenweis, 2002]. The 13–20% diameter underestimate, or 35–50% volume underestimate for the silica spheres constitutes an upper bound of error estimate. The DC-8 sampled a wide variety of natural and anthropogenic aerosol types including urban/industrial pollution and biomass burning from Alaskan/Canadian forest fires during INTEX-NA. The mass was generally dominated by sulfates and organic carbon [Clarke *et al.*, 2007] such that the real part of refractive index is likely to lie between the PSL and silica. Therefore the OPC derived volume may underestimate the actual by about 20%. Apart from this possible bias in estimated mass, the high correlation with the independent direct measurement demonstrates the OPC's consistent performance throughout the experiment. This assures that our data set captures variation in the aerosol mass to extinction ratio with aerosol properties and meteorological conditions.

#### 4. Wavelength Dependence of Ambient Scattering Coefficient

[16] Aerosol number and size, from which mass may be derived, cannot be uniquely determined by light reflectance measured at one wavelength alone. Most satellites detect at multiple wavelengths in order to provide additional constraints. We wish to establish the ambient aerosol multi-

wavelength optical properties from the aircraft data in order to assess the satellite capability in estimating the aerosol mass from spectral radiances. The first step is to estimate the wavelength dependence of ambient scattering coefficient at various altitudes. The wavelength dependence is usually expressed as Ångström exponent ( $\text{\AA} = -\text{dlog}(\sigma)/\text{dlog}(\lambda)$ , where  $\sigma$  is the scattering, and  $\lambda$ , the wavelength).  $\text{\AA}$  is often near 1–2 for small particles (e.g., fresh pollution under dry conditions) and near 0 for large particles (e.g., mineral dust or sea salt).

[17] Although dry scattering was measured at three wavelengths aboard the aircraft, the scattering at higher RH was measured at a single wavelength (near 540 nm) to get  $f(\text{ambRH})$ . The ambient Ångström exponent,  $\text{\AA}_{\text{amb}}$ , was not measured. Instead, we modeled this wavelength dependence using the measured dry size distribution and  $f(\text{ambRH})$ , as described below. The result helps to reconstruct the column AOD at multiple wavelengths (section 5.2) and is evaluated against independent ground measurements (section 5.3).

[18] In order to model humidity growth, aerosol diameters were increased by the aerosol growth factor,  $g(\text{RH})$ , that ranges from 1 to 2 with an increment of 0.01. Subsequently, we used Mie theory and a volume-weighted average of the dry aerosol refractive index (1.59) and the refractive index of water (1.33) to compute ambient aerosol optical properties at three wavelengths for each OPC distribution. These were averaged for 30–45 s during the horizontal flight legs. The ratio of the scattering coefficients calculated from each OPC distribution to the dry value yielded  $f(\text{RH})$ .

[19] Figure 2 compares the Ångström exponent between the humidified (i.e., simulated) and dry (i.e., measured) aerosols. As expected, data points lie near the 1:1 line for low  $f(\text{RH})$  values. Larger  $f(\text{RH})$  values reduce  $\text{\AA}$  from the dry conditions. This reduction in  $\text{\AA}$  is most pronounced when  $\text{\AA}_{\text{dry}}$  takes large values. The dependency of scattering upon wavelength and size is consistent with Mie theory. An undesirable consequence is that  $\text{\AA}_{\text{amb}}$  is less sensitive than

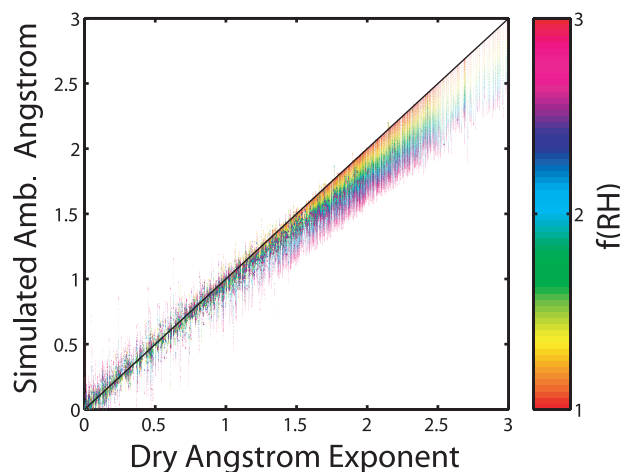


**Figure 2.** Ambient Ångström exponent simulated with the measured aerosol size distribution and sorted with scattering ratio,  $f(\text{RH})$ . When scattering coefficients are converted from dry conditions to ambient, the wavelength dependence is generally reduced, particularly for large  $f(\text{RH})$  and dry Ångström exponent values.

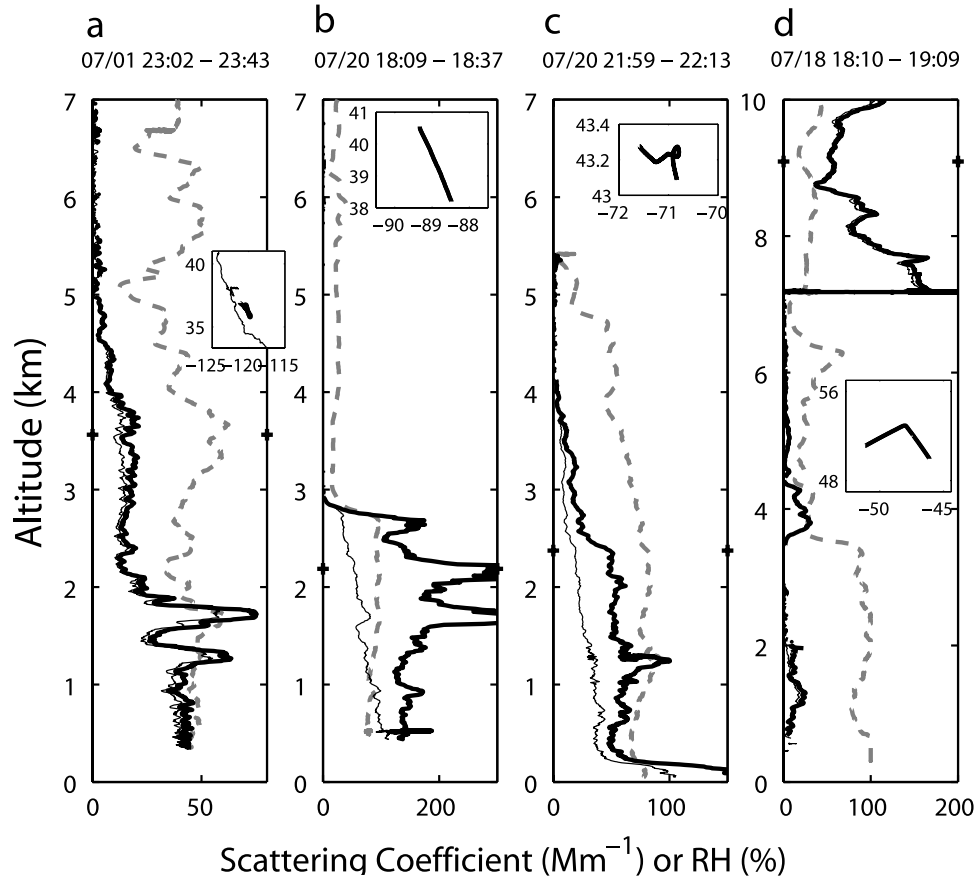


**Figure 3.** Selected vertical profiles of dry (thin solid curve) and ambient (thick solid curve) scattering coefficients along with the measured ambient RH (dashed curve). Plus signs on the vertical axes indicate the altitude of 80% ambient AOD contribution. A map of the flight track is inserted for each profile.

$\dot{A}_{\text{dry}}$  to the dry aerosol size distribution, weakening satellite's ability to employ wavelength dependencies to derive dry aerosol mass. Here we simulate  $\dot{A}_{\text{amb}}$  calculated from our measured  $f(\text{ambRH})$  (adjusted to the ambient RH using equation (1)) and  $\dot{A}_{\text{dry}}$ . A regression line for any simulated  $f(\text{RH})$  value passes through the dry and ambient Ångström exponent coordinates of (0.4, 0.4). As a result, the simulation result was approximated with a polynomial fit.

$$\begin{aligned} \dot{A}_{\text{amb}} = & (-0.022 * f(\text{RH})^3 + 0.16 * f(\text{RH})^2 - 0.47 * f(\text{RH}) \\ & + 1.3) * (\dot{A}_{\text{dry}} - 0.4) + 0.4 \end{aligned} \quad (2)$$

[20] The  $\dot{A}_{\text{amb}}$  calculated with this equation is correlated with the simulated  $\dot{A}_{\text{amb}}$  with a slope of 0.99 and an  $R^2 > 0.99$ . This result is not sensitive to the choice of refractive index. For distributions with small or large Ångström exponents, reducing the refractive index from 1.59 to 1.51–0.01i results in just a 1% larger  $\dot{A}_{\text{amb}}$  even for  $f(\text{RH})$  as large as 3.

## 5. Vertical Profiles and Aerosol Optical Depth

[21] Our goal is to examine the variation of column integral optical properties over the continental United States, the influence of water uptake upon them and their relationship to the effective dry aerosol mass concentration

( $\text{PM}_{2.5\text{proxy}}$ ) measured in the boundary layer. We will relate these to two satellite products, column AOD and its wavelength dependence. The latter are established below using the ambient scattering coefficients derived on a layer basis in the previous section. Where available the results are compared to ground-based observations to check the overall consistency of this approach.

### 5.1. Vertical Profiles

[22] For the column AOD calculation we selected 72 aircraft ascending and descending profiles that spanned at least between 500 and 5000 m, some including portions of horizontal in-progress flight legs. We exclude several profiles where (1) more than 20% of the optical depth is due to aerosols at altitudes above the aircraft altitude according to the LIDAR data or (2) when profiles included data more than 200 km away from the lowest altitude. Shown in Figure 3 are four examples of the profiles. The ambient scattering coefficient at 550 nm is given as the product of dry scattering coefficient and  $f(\text{ambRH})$  adjusted with equation (1) for the ambient RH.

[23] 1. On 1 July, 2302–2343 UTC (Figure 3a) over the Central Valley of California, the winds were northwesterly up to 2 km and southerly 3–5 km. The ambient RH varied between 40 and 60%. Back trajectory analysis [Fuelberg *et al.*, 2007] indicates that the air above 5 km had traveled in

the free troposphere over the Pacific Ocean for one week, keeping the aerosol concentration low.

[24] 2. On 20 July, 1809–1837 UTC (Figure 3b) over Illinois, the boundary layer and free troposphere were separated by a strong inversion. A trough over the east coast and a strong ridge over the Rocky Mountains produced northwesterly winds in the free troposphere. The back trajectories show that the air had traveled over the Pacific Ocean and Canada without nearing the surface for a week prior. The aged boundary layer air up to 2900 m trapped local pollutants, and the very high RH (75–98%) grew them to scatter effectively. The measured aerosol number counts did not rise, confirming that possible droplet shatter of clouds at the inlet did not increase the scattering coefficient.

[25] 3. On 20 July, 2159–2213 UTC (Figure 3c) over New Hampshire, the planetary boundary layer was not distinct from the free troposphere. Westerly/northwesterly winds from Pacific Ocean through Canada and Great Lakes prevailed over the free troposphere. A humid shallow boundary layer below 200 m embedded in southerly winds from the U.S. east coast accounts for moderate aerosol scattering near the surface.

[26] 4. Figure 3d shows a special case where a thick plume of biomass burning aerosol resided in the upper troposphere (7–10 km) on 18 July, 1810–1909 UTC. The midtroposphere and boundary layer were influenced by westerly winds traveled over Great Lakes and slow flow from northwest Canada, respectively. This air mass experienced limited dilution due to swift transport from its origin at the surface over Alaska several days prior.

[27] Most of the observed profiles had similar structures to either one of the first three cases where local pollution is trapped in the boundary layer while the free troposphere contains aerosols transported long-range from other sources. The enhanced upper troposphere plume shown in the last panel is not representative of profiles observed on other days during the experiment.

## 5.2. AOD Estimate and Uncertainty

[28] Most satellites generate column aerosol products such as AOD. Consequently, the first step in the analysis was to characterize the column AOD for the 72 INTEX-A profiles. The AOD at 550 nm is dominated by the vertical integral of the ambient scattering coefficient derived from the nephelometer measurements, such as those shown in Figure 3. The scattering coefficients at 440 and 675 nm were simulated using the ambient Ångström exponent calculation in section 4. The final AOD profiles account for light attenuation due to absorption based on the assumption that the measured absorption coefficient applies to ambient conditions [Nessler *et al.*, 2005]. Occasionally, we interpolated over layers without aircraft measurements. For the altitudes with no absorption measurement, we assumed the experiment-wide average single scattering albedo (SSA), which decreased from 0.96 near the surface to 0.88 at 6 km at 550 nm.

[29] The AOD contributed by the altitudes lower than the lowest aircraft altitude (500 m or lower) was assumed to be equal to that of the layer of the same thickness immediately above it multiplied by a pressure adjustment factor. The factor accounts for the atmospheric pressure gradient with

altitude and ranged between 1 and 1.06. Because pollution sources are at the surface, the scattering coefficient can be higher than this well mixed assumption as you approach the surface (see Figure 3c for example). Hence in a poorly mixed near-surface layer, this assumption may bias the estimated AOD toward low values.

[30] The extinction coefficient due to the aerosols in the troposphere above the highest altitude flown by the DC-8 (>5 km to 10 km) was assumed to be the experiment-wide mean of 2.7, 2.0, 1.6  $\text{Mm}^{-1}$  at 450, 550 and 700 nm, respectively. We also assume here that the lowest 5% of AOD values measured by the J31 between 5 and 7.5 km reflect a clean upper troposphere and are representative of stratospheric AOD. This stratospheric AOD was identified to be 0.014, 0.0077 and 0.0053 at 440, 550 and 675 nm, respectively. These values were estimated using differential AOD measured from the J31 aircraft [Russell *et al.*, 2007] during the INTEX-A over the U.S. east coast. This stratospheric AOD accounts for 20% or less of the total ambient AOD for most profiles.

[31] Unusually low or high AOD values were excluded by focusing on the center two thirds of our observations. Uncertainty in the estimated ambient column AOD ranges over 16–46% for this data, with a median value of 23%. It originates primarily from the  $f(\text{RH})$  measurement and the contribution from near-surface layer. The scattering increase from the dry to ambient RH conditions is subject to the errors in  $\gamma$  and ambient RH measurements. Assuming a 4% uncertainty in the RH measurement and 5% in the Radiance Research nephelometer scattering measurement, equation (1) provides  $\gamma$  to an accuracy of <14% for this data. This translates into <15% uncertainty in  $f(\text{RH})$ . Doubling and halving the estimated extinction in the near-surface layer below the minimum aircraft altitude results in median ambient AOD changes by +12% and –6%, respectively.

[32] Minor sources of error include the dry scattering measurement noise (<1  $\text{Mm}^{-1}$ , compensated for when integrated over the altitudes), the truncation correction (~4% for no-impactor-cut samples, less for submicron [Anderson and Ogren, 1998]), absorption (2%, discussed in section 2) and the aerosol AOD in the upper troposphere (in the order of 0.01).

## 5.3. AERONET Comparison

[33] Profiles over AERONET sites [Holben *et al.*, 1998] provided an opportunity to evaluate our calculated column AOD. The estimated AOD is compared here with AERONET level 2.0 data that has been pre and post field calibrated, automatically cloud cleared and manually inspected. Three of the INTEX-NA vertical profiles met our selection criteria that the aircraft at its lowest altitude was located within 100 km of the AERONET site and that the AERONET site was under clear sky within 4 hours (equivalent to 100 km at a wind speed of 7 m/s) of the aircraft/AERONET measurements being compared. These large spatial and temporal differences make the comparison less precise than coordinated aircraft spiral ascents/descents over the ground sites. However, the comparison is valuable in demonstrating the general consistency in our estimate of AOD and its wavelength dependency.

[34] The ambient AOD shows reasonable agreement with AERONET AOD data for the three vertical profiles

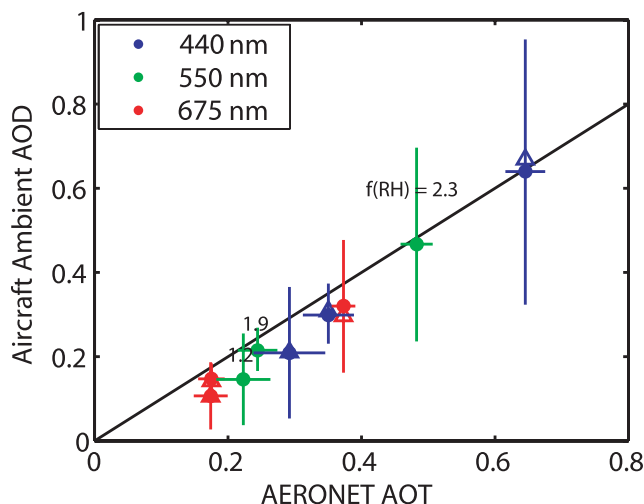


**Figure 4.** Ambient AOD derived from the aircraft measurements of scattering and  $f(RH)$  compared with the AERONET measurements at 440 nm (blue circles), 550 nm (green circles) and 675 nm (red circles) for the first three profiles of Figure 3. The triangles indicate the result of ignoring wavelength dependence of scattering increase. The bars indicate temporal and spatial variances observed by AERONET and aircraft LIDAR, respectively, in addition to the measurement uncertainty.

(Figure 4). The horizontal bars indicate one standard deviation of the AERONET 15-min-average AOD within  $\pm 4$  hours of the aircraft overpass. In order to assign a measure of variance to the aircraft AOD profile, we assume the variance in AOD is similar to that evident in the vertical integral of the lidar backscatter taken within 100 km of the AERONET site. The product of this coefficient of variance and the AOD from the profile provides an estimate of aircraft AOD variance for all wavelengths. The vertical bars in Figure 4 indicate this spatial and temporal variance as well as the measurement uncertainty.

[35] The poorest agreement between calculated and observed ambient AOD occurs for the lowest AOD values which were measured at the Fresno California AERONET site ( $36.8^{\circ}\text{N}$ ,  $119.8^{\circ}\text{W}$ ) on 1 July, 2302–2343 UTC (Figure 3a). Cirrus clouds may have been present near 10700 m in the vicinity of the ground site. The aircraft data shows that, while the scattering coefficient at this altitude remained below the detection limit, the ambient RH exceeded 95%. The highest AOD was measured at the Bondville, Illinois AERONET site at ( $40.1^{\circ}\text{N}$ ,  $88.4^{\circ}\text{W}$ ) on 20 July, 1809–1837 UTC (Figure 3b). The lidar found a high spatial variability of aerosol scattering, resulting in the long vertical error bar. The variance estimates from the AERONET data (horizontal bars) indicate that clouds did not affect the measurements or were effectively removed. This profile with the highest  $f(\text{ambRH})$  value highlights the application of our Ångström exponent modeling. If we ignore the wavelength dependence of  $f(\text{ambRH})$  for this high-humidity case, the calculated AOD deviates from the best estimate by +0.03 (+5%) at 440 nm and −0.02 (−7%) at 675 nm (triangles in Figure 4). Incorporating the wavelength dependence of  $f(\text{ambRH})$  into the ambient AOD

calculation results in only marginally better agreement with the AERONET direct measurements.

[36] These comparisons do not represent “closure” studies. However, the agreement demonstrates the general validity of our approach for obtaining ambient AOD and its wavelength dependency. Where concurrent airborne and ground based measurements of column AOD can be more effectively compared over appropriate spatial and temporal scales, we expect that differences would be smaller than those presented here and mainly reflect nonideal instrument behavior and uncertainties in the aerosol properties such as size distribution, refractive index, and hygroscopicity. We note that even deliberate in situ closure profiles for AOD evaluations are expected to yield calculated AOD uncertainties on the order of 15–20% [Redemann *et al.*, 2003].

## 6. Mass Estimate and Local Mass Scattering Efficiency

[37] Here we estimate aerosol density and PM<sub>2.5</sub> mass in the boundary layer. The aerosol mass and extinction is linked in the local domain, before extending our scope to the vertical column in next section.

[38] Aerosols in the boundary layer were predominantly of urban origin. Biomass burning events identified using measured gas concentrations were mostly found in the free troposphere [Clarke *et al.*, 2007], with limited influence on the mass-scattering relationship in the boundary layer. Also, we do not find any air mass where aerosol sizes up to  $2.5\ \mu\text{m}$  were dominated by dust.

[39] The limited contribution of biomass burning and dust plumes relative to regional pollution justifies the use of a single density value for the size distributions in the boundary layer in our selected vertical profiles. Previous DMA measurements made for urban aerosols in Atlanta resulted in a density range of  $1.54\text{--}1.77\ \text{g/cm}^3$  [McMurry *et al.*, 2002]. The variability of this density estimate is less than  $\pm 10\%$ . We use a value of  $1.7\ \text{g/cm}^3$  and estimate an uncertainty associated with the choice of density at 15% considering that Atlanta may not represent the U.S. nation-wide urban pollution. Clarke *et al.* [2007] estimated mass of ions, organic compounds and black carbon using chemical mass and size distribution measurements during INTEX-NA. Their density for most of the urban pollution samples falls in  $1.5\text{--}1.7\ \text{g/cm}^3$ , to further support our choice of density in the present paper. We do not estimate the aerosol mass of biomass burning or dust in the troposphere, or column integral mass.

[40] PM<sub>2.5</sub> mass was approximated by this density times the integral over  $0.1\text{--}1.9\ \mu\text{m}$  of OPC volume distribution taken at  $500 \pm 200\ \text{m}$  above sea level (PM<sub>2.5, \text{proxy}}</sub>). This upper size cut roughly corresponds to an aerodynamic diameter upper limit to  $2.5\ \mu\text{m}$  for the assumed particle density. The volume integral is weakly sensitive to the upper cut size unless there is a large relative volume in the coarse mode. Cut at  $2.4\ \mu\text{m}$  instead, the volume is higher only by a maximum of 3% for 95% of the samples. The largest particles can also suffer from inertial collision into the inner wall of inlet, resulting in undercounting. However, the loss is considered negligible for aerodynamic sizes of  $2.5\ \mu\text{m}$  and below [McNaughton *et al.*, 2007]. The particle size measured with the OPC is sensitive to the

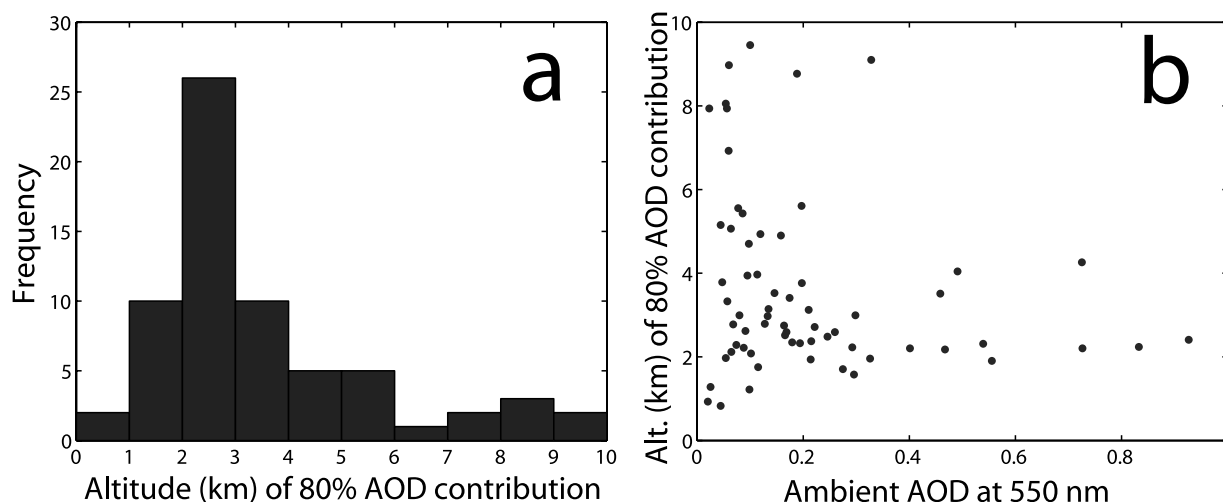


**Figure 5.** (a) Frequency of height up to which 80% of ambient column AOD exist. (b) The 80% AOD height and ambient AOD. A data point with AOD and altitude of 1.4 and 1.6 km is omitted.

refractive index, which may result in a mass underestimate of about 20% (section 3). The 15% uncertainty in density discussed above brings the overall  $\text{PM}_{2.5\text{proxy}}$  uncertain range to  $-15\%$  and  $+25\%$  (lower and upper limits). Furthermore, we emphasize that size distributions measured at our lowest altitudes of  $500 \pm 200$  m may not reflect surface concentrations when strong near surface gradients exist. Despite these limitations, the estimated  $\text{PM}_{2.5\text{proxy}}$  remains useful in estimating correlation between the dry aerosol mass and the column optical properties as well as in sorting their relationship with relative humidity and wavelength dependence of light extinction.

[41] The regression between the measured aerosol volume and scattering at an altitude of 500 m yielded the expression Dry Volume ( $\mu\text{m}^3/\text{cm}^3$ ) =  $0.076 \times \text{Ambient Scattering Coefficient (Mm}^{-1}) + 1.8$ , and gives a root square mean volume difference of  $1.8 \mu\text{m}^3/\text{cm}^3$  while the volume ranged between 0 and  $20 \mu\text{m}^3/\text{cm}^3$ . The  $R^2$  is 0.86 for all cases under ambient RH of 90% or lower. This robust relationship is consistent with the observation that aerosols in the boundary layer were predominantly of urban origin.

[42] The ambient scattering coefficient per dry  $\text{PM}_{2.5}$  mass is  $5.0 \pm 2.2 \text{ m}^2/\text{g}$  (mean and one standard deviation), and the ambient extinction per dry  $\text{PM}_{2.5}$  mass centers at  $5.3 \text{ m}^2/\text{g}$ . The dry scattering per dry  $\text{PM}_{2.5}$  is  $3.6 \pm 1.3 \text{ m}^2/\text{g}$ . Mass scattering and extinction efficiencies (MSE and MEE, respectively) for total aerosols (not truncated at  $2.5 \mu\text{m}$  aerodynamic) are expected to be slightly lower than these values, but are not available owing to the lack of a reliable measurement of coarse mode size distribution and total mass.

[43] Our submicron MEE estimated at 55% RH for our dry OPC volume is  $4.6 \pm 1.4 \text{ m}^2/\text{g}$  in the boundary layer, and close to previous ship measurement for North America's boundary layer aerosol of about  $3.7 \pm 1.3 \text{ m}^2/\text{g}$  at 55% RH [Quinn and Bates, 2005]. Even closer agreement was found for this parameter between our optical techniques and the latter for the INDOEX data [Clarke et al., 2002]. The possible volume underestimate of about 20% mentioned earlier in section 3 would only improve the overlap between these values. The submicron MEE is the scatter-

ing coefficient measured behind an impactor with a 50% cut size of  $1 \mu\text{m}$  aerodynamic, adjusted to an RH of 55% using the measured total  $f(\text{RH})$ , increased by the dry submicron absorption coefficient and divided by the dry OPC aerosol volume integral up to  $0.75 \mu\text{m}$  (equivalent to  $1 \mu\text{m}$  aerodynamic) and a density of  $1.7 \text{ g}/\text{cm}^3$ . This falls into the range of submicron MEE for non-sea-salt sulfate aerosols ( $2.9\text{--}5.3 \text{ m}^2/\text{g}$ ) and particulate organic matter ( $4.4\text{--}7.6 \text{ m}^2/\text{g}$ ), observed over Indian and Atlantic Oceans by Quinn et al. [2002].

[44] A similar variance is associated with the dry submicron MEE computed for a refractive index of 1.59 from our OPC size distribution instead of the nephelometer measurement:  $4.1 \pm 1.3 \text{ m}^2/\text{g}$ . This is a result of moderate variation in the shape of size distribution. The effective diameter (volume/area\*6) of the total distribution (including coarse mode) varied between  $0.26$  and  $0.57 \mu\text{m}$  for the center two thirds of our data.

## 7. Discussions

### 7.1. Altitude of 80% AOD Contribution

[45] Because both water vapor and aerosols originate at the planetary surface we expect higher ambient scattering coefficient at the surface and within the planetary boundary layer than in the free troposphere. This has been shown to be the case in clean marine conditions [Shinozuka et al., 2004]. However, wet and dry convective events can inject both gas phase secondary aerosol precursors (e.g.,  $\text{SO}_2$ ) and primary aerosols (e.g., soot, biomass smoke) into the free troposphere especially during summer in North America. These high scattering layers are often only hundreds of meters thick but are hundreds of kilometers in horizontal extent, and difficult to observe from satellites or to predict using chemical transport models.

[46] In order to evaluate the range of altitudes that dominate AOD over North America we identify the altitude below which column extinction accounts for 80% of the total column AOD. This is plotted as a histogram in Figure 5a for all INTEx-A profiles, and is shown as plus signs on the vertical axis of the profiles in Figure 3. Its

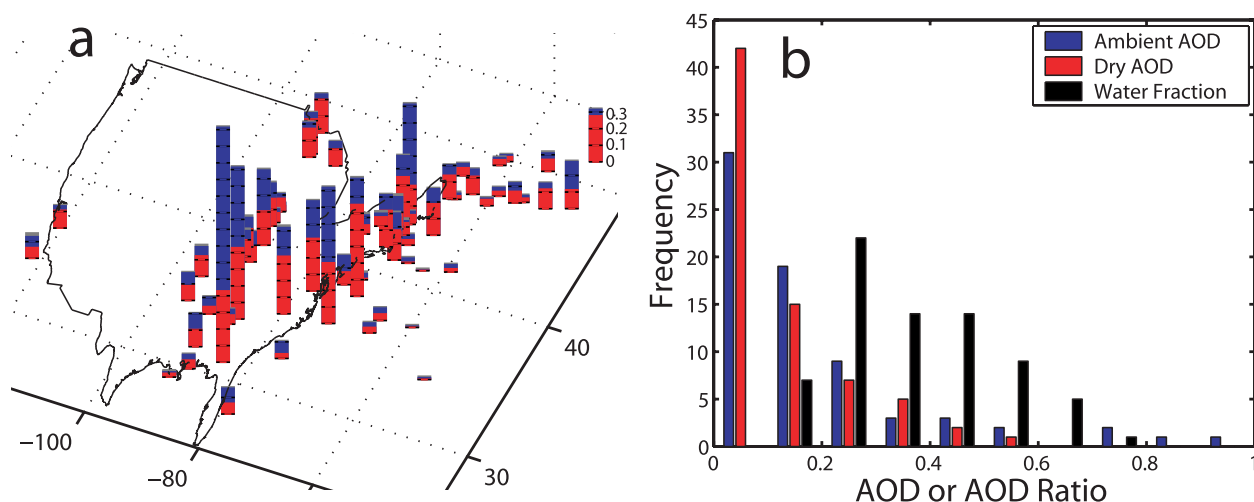


**Figure 6.** (a) Dry (red) and ambient (blue) AOD pictured over the measurement locations. Each bar represents a vertical profile flown in the summer of 2004. Grey bars indicate the estimated fraction of AOD contributed from the altitudes above DC-8 coverage (upper free troposphere and stratosphere). The tick has a 0.1 increment. (b) Frequency of dry (red) and ambient (blue) AOD. The light extinction for altitudes above DC-8 coverage is not included. One data point, an ambient AOD of 1.4, is not shown. The black bars indicate one minus their ratio, or the water fraction.

uncertainty is mostly driven by the  $f(RH)$  error (discussed in section 5.2) and has a median of  $-24\%$  and  $+48\%$  for positive and negative  $f(RH)$  excursion, respectively. A smaller ( $\sim 5\%$ ) uncertainty results from the lack of measurements below 500 m. Of the 72 profiles, 38 (53%) have more than 80% of the total column AOD below 3000 m, and 53 (74%) below 5000 m. This is usually due to natural and anthropogenic aerosols generated and trapped within the boundary layer as shown in Figures 3b and 3c. We note that in a few cases, pollution from remote sources may have subsided into boundary layer after being transported in the free troposphere [Clarke *et al.*, 2007]. Figure 3a is a variant of this type. In this case, pollution in the boundary layer ( $<2.0$  km) led to moderate scattering coefficients, but relative humidity was low. Air transported from the south in the free troposphere below 5 km was also influenced by anthropogenic aerosols at moderate (50%) relative humidity. This led to an 80% AOD altitude of 3.6 km illustrating the importance not only of high aerosol loading but the influence of relative humidity on AOD. AOD larger than 0.4 were generally associated with high scattering near the surface up to 2.5 km (Figure 5b) primarily due to high aerosol loading and RH.

[47] There are three exceptions to these general features, all of which occurred on 22 July. During this flight total aerosol scattering reached values as high as  $300 \text{ Mm}^{-1}$  in biomass burning plumes near 4 km. Even in these cases, the boundary layer contributed most of the AOD. These biomass burning plumes were dry ( $\sim 20\%$  RH) and contributed little more than 20% of the total column ambient AOD. The dry scattering values were near  $100 \text{ Mm}^{-1}$  in the boundary layer, but because of high RH the ambient scattering exceeded  $\sim 200 \text{ Mm}^{-1}$  accounting for almost 80% of the total column AOD.

[48] Layers with elevated scattering values were observed occasionally at high altitudes on other days but did not result in a large column AOD enhancement. On 18 July

(Figure 3d), the biomass plume from Alaskan/Canadian forest fires traveled across the continent to northeastern Canada, and exhibited a fractional AOD of 0.26 between 7 and 10 km over an otherwise clean marine column (AOD up to 7 km was 0.06). The water uptake was negligible in the dry (ambient RH near 30%) layer thus the column AOD was driven solely by the high aerosol loading aloft. The 18 and 22 July profiles are exceptional but forest fire plumes were not randomly sampled as flights were directed to their location in order to study them.

## 7.2. AOD and Its Water Fraction Over the Continental United States

[49] Here we describe general features of AOD observed over the U.S. mainland, and discuss its variation in terms of the two most important factors, hygroscopicity (related to chemical components) and ambient RH (driven by meteorology) for the given dry aerosol concentration (related to  $\text{PM}_{2.5}$ ). This assessment is expected to provide input to regional aerosol models that compute the optical properties such as ambient AOD, and to assess remote sensing capability in estimating dry AOD and  $\text{PM}_{2.5}$ . The AOD variation is discussed again in section 7.4 in relation with the boundary layer aerosol mass.

[50] Ambient AOD estimated for the vertical profiles (section 5.2) are plotted over the continental U.S. map for all times during the experiment in the summer of 2004 (Figure 6a). Red bars illustrate the dry aerosol scattering integrated over the altitudes (dry AOD) without applying humidity growth rate. The difference (blue bars) indicates the AOD attributed to water uptake. We define the water fraction of AOD,  $W_f$ , as

$$W_f = 1 - (\text{dryAOD}/\text{ambientAOD}) \quad (3)$$

[51] The frequency of dry and ambient AOD and  $W_f$  are shown in Figure 6b. Note that individual profiles in the

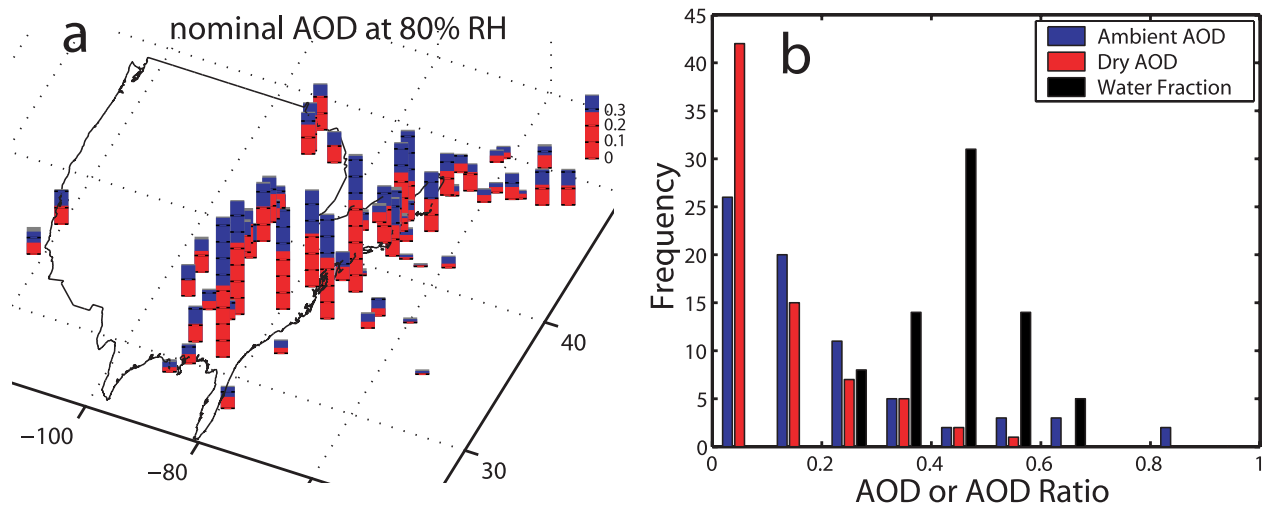


**Figure 7.** Same as Figure 6 except that the ambient AOD is simulated for a constant RH of 80%.

figure are not statistically representative of a specific area, season, meteorology or any other conditions. Local weather alone exposes aerosols to a variety of mixing, transport and humidity conditions that may result in higher variance in AOD and Wf than what the experiment experienced.

[52] AOD is 0.3 or lower for most cases, and are generally lower over the ocean than over the land, primarily because of air mass type and proximity to sources. However, the air over the ocean off the northeastern Canada and further east was affected by some pollutants which were brought by southwesterly winds from New England and other areas. In contrast, south of about 40°N and away from the land we only encountered small AOD. Two of these profiles sampled outflow that had passed over Pennsylvania. The ambient scattering coefficient was moderate near 50  $\text{Mm}^{-1}$  in 1–2 km, but dropped to  $\sim 20 \text{ Mm}^{-1}$  at lower altitudes. This suggests that pollutants from the land had been scavenged in the boundary layer or lifted up over cleaner and cooler air. In the other two profiles, the air had circulated over the ocean for at least a week prior to the measurement at all levels, and carried few pollutants.

[53] The AOD over land does not show a clear trend with reference to location, because aerosol sources are closer and transport patterns are more complex than over the ocean (section 5.1). In one profile (the tallest bar in Figure 6a; omitted in Figure 6b) the ambient AOD was 1.4 due in part to high ambient RH (>90%). Under different wind and humidity patterns the AOD is often lower than 0.1 in this vicinity.

[54] The water fraction varied widely. The high-elevation forest fire aerosols over northeast Canada (Figure 3d), for example, were weakly hygroscopic with little water contribution to AOD (12%), as is indicated by the almost completely red bar located at the far right. The estimated Wf is a function of  $\gamma$  and ambient RH. These two parameters could positively correlate with each other, if, for example, aerosols had been dominated by sea salt (hygroscopic particles often found in humid air) or dust (hydrophobic particles often found in dry air). For an analysis later it is important to realize that these two factors were found independent for the INTEX-NA data.

[55] One way to demonstrate the relative importance of ambient RH versus physiochemistry ( $\gamma$ ) to the ambient AOD is to simulate the ambient AOD with a fixed ambient RH (say at 80%). The result (Figure 7a) illustrates how much AOD variation is driven by that of  $\gamma$  independent of ambient RH variation. The unusually high ambient AOD case in Figure 6 shows a reduced but still large percentage due to water. Wf (Figure 7b) takes a narrower range of values,  $0.46 \pm 0.11$  (mean and one standard deviation) at 80% RH, than the same parameter simulated with the observed RH ( $\text{Wf} = 0.37 \pm 0.15$ , Figure 6b). Wf simulated for other fixed ambient RH values shows similarly narrower distributions (Figure 8). These express the degree by which knowing ambient RH can improve estimates of dry-ambient AOD. There are differences in Wf among the profiles for a given RH. Realistic values of hygroscopicity (determined primarily by chemistry and size distribution) are essential in modeling the ambient AOD and in retrieving dry AOD to 10% or better.

### 7.3. Model and Satellite Retrieval Accuracies

[56] So far we have used the measured aerosol dry scattering, its humidity response and the ambient RH to establish ambient AOD. Below, the ambient AOD is recalculated with reasonable uncertainties in the input variables. We claim that the ambient AOD sensitivity revealed from this test can be scaled with error associated with input of  $\gamma$  in regional aerosol models. Satellite retrieval of aerosol water fraction and PM<sub>2.5</sub> may suffer a similar limitation.

[57] Values of  $\gamma$  are rarely available, particularly because of the poorly known influences from organic carbon (OC) fractions [Quinn *et al.*, 2005]. Clarke *et al.* [2007] found  $\gamma$  to vary by  $\pm 0.1$  or less for a given OC fraction. We assume here, for the sake of a sensitivity test, that the regional aerosol models can generate  $\gamma$  values to  $\pm 0.1$  provided they resolve the OC fraction. An increase in  $\gamma$  ( $\Delta\gamma$ ) by 0.1 in equation (1) results in a 3–21% (median 9%) increase in the ambient AOD ( $\Delta\text{AOD}$ ) depending on the vertical profile considered and the associated ambient RH (dots in Figure 9). If  $\Delta\gamma$  remains near or within  $\pm 0.1$ ,  $\Delta\gamma$  and  $\Delta\text{AOD}$  are almost linearly correlated with each other. Similarly, an increase from the observed ambient RH by 5 and 10 percentage points

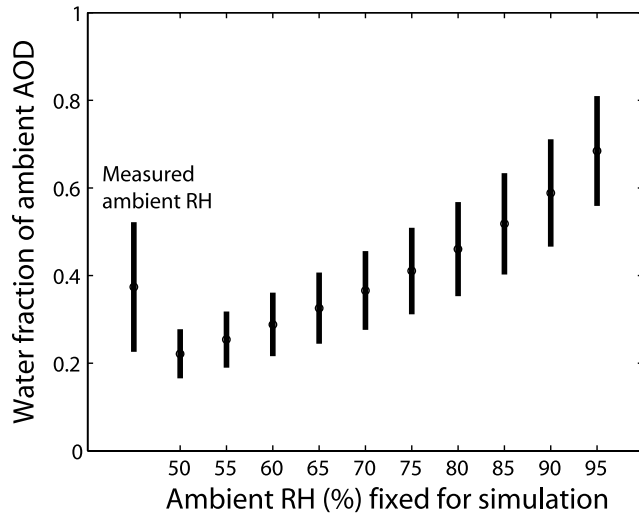


**Figure 8.** Mean and standard deviation of water fraction simulated for the 72 INTEX-A vertical profiles with the measured and fixed RH. Knowing the ambient RH reduces the error in translating remotely sensed single-wavelength ambient AOD into dry AOD, particularly under low RH associated with shorter bars.

(without any variation in  $\gamma$  imposed) results in an increase in the median ambient AOD of 11% (not shown) and 26% (circles), respectively.

[58] The error in the ambient RH and  $\gamma$  need to be minimized for a model to maintain an uncertainty in the ambient AOD similar to that claimed in the MODIS AOD observation over land ( $\pm 0.05 \pm 0.15 \times \text{AOD}$  [Remer et al., 2005]). Using a simulation with ambient RH increased by 10 percentage points for the measured  $\gamma$ , about two thirds of the 72 profiles lie within the uncertainty in the MODIS best estimate of AOD over land. If the model  $\gamma$  is overestimated by 0.1, then the column effective ambient RH has to be

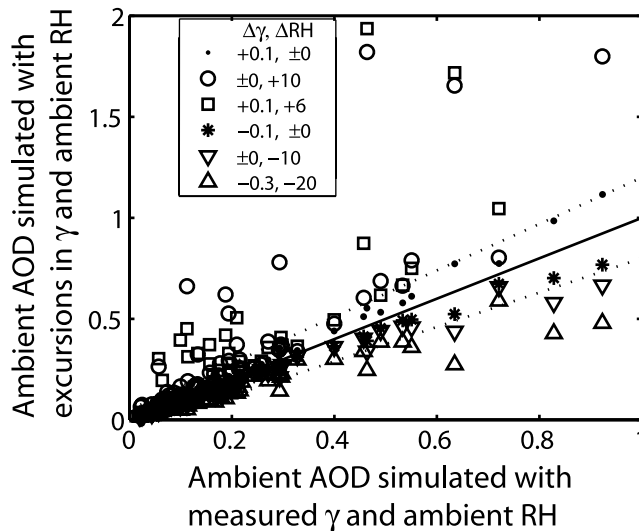


**Figure 9.** Ambient AOD simulated with excursion in  $\gamma$  and ambient RH for sensitivity test. The dashed curves indicate the nominal uncertainty in MODIS AOD observations over land.

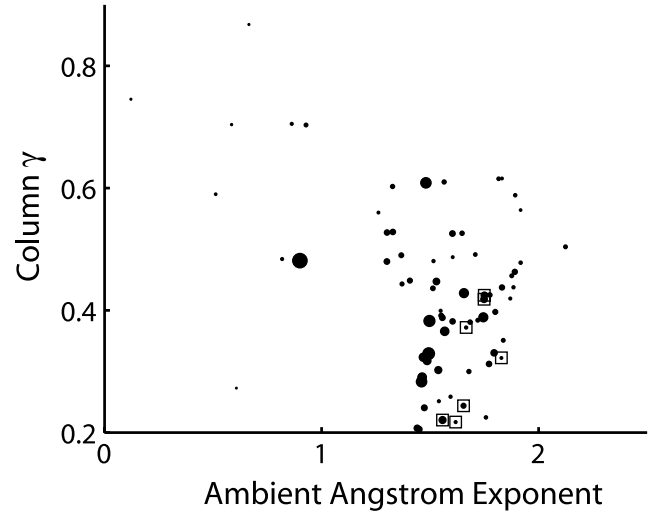


**Figure 10.** Column average  $\gamma$  compared to the Angstrom exponent of ambient AOD. Dot size is proportional to the ambient AOD. Squares indicate the 18 July data.

known to  $\sim 6$  percentage points (squares in Figure 9) in order to maintain similar uncertainties. Downward bias in the input variables is less critical: Even if  $\gamma$  and RH are underestimated by 0.3 and 20%, respectively, most data, those with small AOD in particular, remains within the MODIS uncertainty.

[59] For remote sensing, the length of the vertical bars in Figure 8 provides the expected ranges of uncertainty in translating ambient AOD into dry AOD without using a spectral dependence: These are 15% of the ambient AOD, or 6–13% when the RH is known. Using multiple wavelength remote sensing does not help to constrain either  $\gamma$  or water fraction. Figure 10 compares column  $\gamma$  with the Ångström exponent of the ambient AOD. The marker size is proportional to the ambient AOD at 550 nm to better identify measurements with a high signal-to-noise ratio. The 18 July data partially affected by the biomass burning plume (squares), for example, show a weakly positive correlation expected for the mixture of biomass burning and urban pollution (low to high change in Ångström exponent and hygroscopicity). However, the relationship between these two parameters is not well defined for the entire experiment. This holds true for a comparison between the water fraction and Ångström exponent (not shown) as well. The Ångström exponent takes a rather narrow range of values, while the various mixture of organic (not hygroscopic) and inorganic (many species of them being hygroscopic) material results in a wide variation in hygroscopicity.

#### 7.4. PM<sub>2.5</sub><sub>proxy</sub> Versus AOD

[60] As mentioned earlier, a relation demonstrated between column AOD and near surface integral dry mass, estimated from our integrated distributions (PM<sub>2.5</sub><sub>proxy</sub>), would support use of remote sensing to assess PM<sub>2.5</sub> remotely. Our boundary layer PM<sub>2.5</sub><sub>proxy</sub> and column AOD show a linear trend (Figure 11). The geometric mean regression is expressed as  $\text{AOD} = 0.019 \times \text{PM}_{2.5\text{proxy}} (\mu\text{g}/\text{m}^3) + 0.0022$ , with  $R^2$  of 0.77 ( $R^2 = 0.60$  including the outliers). The root mean square of AOD and mass differ-

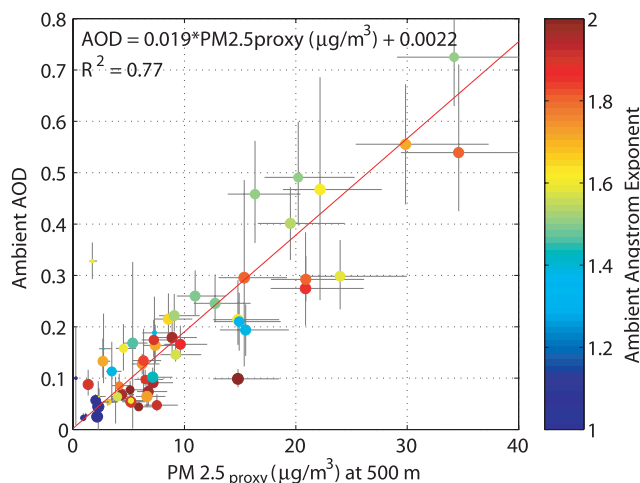


**Figure 11.** Ambient AOD and boundary layer aerosol mass ( $\text{PM}_{2.5\text{proxy}}$ ) for the 72 vertical profiles. The regression line for all but three outliers ( $\text{AOD} > 0.8$ ) is  $\text{AOD} = 0.019 \cdot \text{PM}_{2.5\text{proxy}} (\mu\text{g}/\text{m}^3) + 0.0022$ ,  $R^2 = 0.77$  ( $R^2 = 0.60$  including the outliers). Small dots indicate profiles with high altitude of 80% AOD contribution, and the color indicates ambient Angstrom exponent.

ences from the regression line is  $0.076$  and  $3.3 \mu\text{g}/\text{m}^3$ , respectively. The  $R^2$  is lowered from that for the actual mass-AOD correlation by the limited precision of the OPC measurement, evident in the scattering comparison with the nephelometer (see section 3 and Figure 1). Also note that a part of the intercept reflects light attenuation due to particles that do not contribute to the boundary layer mass, such as the stratosphere's AOD ( $0.008$ ). The error bars reflect the estimates made in section 6 for  $\text{PM}_{2.5\text{proxy}}$  and in section 5.2 for the ambient AOD. In particular, the possible 20% mass underestimate discussed in section 3 may lower the slope to  $0.016$ . We emphasize that this regression is only applicable for summertime United States. Application for different seasons or other regions remains to be demonstrated. This figure was made after removing three outliers where ambient  $\text{AOD} > 0.8$ . These outliers were observed near or above clouds. The air was stagnated in two of them, and flowing rapidly eastward in the other. The ambient RH was high ( $>90\%$ ), and the aerosols were hygroscopic, making these distinct from the other data points.

[61] RH variability alone does not explain all of the remaining outliers. The high-elevation biomass burning plume (Figure 3d) manifests itself as a low  $\text{PM}_{2.5\text{proxy}}$  ( $1.7 \mu\text{g}/\text{m}^3$ ) high AOD ( $0.33$ ) case. Since most contribution to AOD was made at  $7$  km or higher, the AOD is least influenced by the boundary layer aerosol mass. Other profiles with high altitudes of 80% contribution are indicated with small dots in Figure 11, and lie among the normal cases with low or moderate AOD. In practice, chemical transport models or satellites with vertical resolution (e.g., CALIPSO) could identify or exclude cases with high-elevation plumes, and increase the predictability of the boundary layer  $\text{PM}_{2.5}$  mass.

[62] Although there is a tendency for higher Angstrom exponents to lie below the line in Figure 11, this parameter helps to constrain the mass  $\text{PM}_{2.5\text{proxy}}$  to AOD ratio only to

a limited extent. A smaller ( $<1.5$ ) ambient Angstrom exponent is generally associated with a larger mass per AOD. Because of generally diverse aerosol types at different altitudes, this relationship is less evident over the column than on a layer by layer basis (not shown). Also, the humidification of aerosols makes the Angstrom exponent less sensitive to changes in the size distribution, as was found in section 4 and Figure 2. Once expanded to a larger number of samples, this approach will give a guideline of the degree to which the use of spectral dependence differentiates the near-surface mass. It remains possible that, in combination with other observable parameters, the wavelength dependence may help improve the remote sensing resolution. However, this investigation using ambient RH, fine mode fraction and location failed to demonstrate this.

[63] Our AOD- $\text{PM}_{2.5}$  relationship overlaps, albeit with a greater slope of regression line, with that found by Wang and Christopher [2003]. They did the comparison on a daily basis with MODIS and ground  $\text{PM}_{2.5}$  data in Jefferson County, AL to find a slope of  $0.014$ . Their results show considerably more scatter. This is expected because of their longer sampling time and because the present study compares the nephelometer derived optical depth with OPC derived volume, whereas their relationship is made with spatially averaged satellite and surface data. Our study also explicitly addresses the role of  $f(\text{RH})$ , as they suggested was needed. The inferred mass is better correlated with the optical properties in our data than it is in the real atmosphere, because we neglect the case by case variations in refractive index and density. The similar trends found by these two independent studies for different locations, timing, measurement techniques and averaging methods provide confidence in the results, and encourages the use of these approaches for inferring  $\text{PM}_{2.5}$ .

## 8. Summary

[64] During the INTEX-North America aircraft campaign, we generated vertical profiles of visible light scattering by dry aerosols and its response to water uptake,  $f(\text{ambRH})$ , over the troposphere. Urban/industrial pollutants and forest fire plumes were found at various altitudes depending on the air stability, winds and scavenging processes prior to the measurements. The  $f(\text{RH})$  was measured at  $550$  nm and its wavelength dependence simulated using the measured size distribution. Applying  $f(\text{ambRH})$  values defined at  $550$  nm to other wavelengths could cause a  $5$ – $7\%$  error at  $440$  and  $675$  nm. The ambient AOD was estimated on the basis of these measurements and simulation, and found consistent with the Sun photometer measurements from ground.

[65] About 80% of the total column AOD was found to be below  $3$  km for 53% of the vertical profiles and below  $5$  km for 74%. Ambient AOD larger than  $0.4$  required both high aerosol loading and high RH, and were always found with high contribution from the surface layer up to  $2.5$  km. Over the U.S. mainland, both the ambient RH and  $\gamma$  are important for determining the water contribution to AOD. Modeling the ambient AOD from dry aerosol size distributions to accuracy comparable to the MODIS AOD determination over land requires input of column effective ambient RH to be known within about 6 percentage points when  $\gamma$  is known to  $0.1$ . Dry AOD inferred from remote sensing

without knowledge of column effective RH has a typical error equivalent to 15% of the ambient AOD. This uncertainty is reduced to 6–13% when the column effective ambient RH is known. The column Ångström exponent exhibited a relatively narrow range (mostly 1.3–1.9), and did not show a trend with the hygroscopicity or the water fraction of ambient AOD, perhaps because of the wide variety of mixing between organic and inorganic material and the negligible concentrations of dust and sea salt. Hence the wavelength dependence of radiances did not help us constrain evaluation of the dry AOD and mass over the continental United States.

[66] Our measured size distribution provided an estimate of boundary layer PM<sub>2.5</sub> dry mass (PM<sub>2.5</sub><sub>proxy</sub>) to a ~25% accuracy. Representative values of PM<sub>2.5</sub><sub>proxy</sub> were compared with column AOD for different aerosol profiles and column effective ambient RH. Ambient AOD correlated well with the boundary layer PM<sub>2.5</sub><sub>proxy</sub> ( $AOD = 0.019 \cdot PM_{2.5, proxy} (\mu g/m^3) + 0.0022$ ,  $R^2 = 0.77$ ) for 96% of the data in spite of the large variations in vertical aerosol structure. This supports the potential application of satellite derived AOD for the inference of near surface PM<sub>2.5</sub>. Removing high-ambient-RH (>90%) high-AOD (>0.8) cases appears more effective than use of the wavelength dependence of radiances to remotely sense PM<sub>2.5</sub>.

[67] **Acknowledgments.** We would like to acknowledge support of part of our team through NASA grant NNG04GB39G and that of Yohei Shinozuka through NASA ESSF/05-0000-0186 for this work. We also thank the NASA DC-8 team at Dryden, California, for their mission support; Henry E. Fuelberg and his colleagues at Florida State University for the back trajectory products; Edward V. Browell and his colleagues at NASA Langley Research Center for the DIAL lidar data; and AERONET Pls Brent Holben, Steve Jones and Carol J. Bruegge for their efforts in establishing and maintaining the Bondville, Billerica, and Fresno sites. We are also grateful to the anonymous reviewers for their helpful comments. This is SOEST contribution 7116.

## References

- Anderson, T. L., et al. (1996), Performance characteristics of a high-sensitivity, three-wavelength, total scatter/backscatter nephelometer, *J. Atmos. Oceanic Technol.*, **13**, 967–986.
- Anderson, T. L., and J. A. Ogren (1998), Determining aerosol radiative properties using the TSI 3563 integrating nephelometer, *Aerosol Sci. Technol.*, **29**, 57–69.
- Chu, D. A., Y. J. Kaufman, L. A. Remer, and B. N. Holben (1998), Remote sensing of smoke from MODIS airborne simulator during the SCAR-B experiment, *J. Geophys. Res.*, **103**(D24), 31,979–31,987.
- Chu, D. A., Y. J. Kaufman, C. Ichoku, L. A. Remer, D. Tanré, and B. N. Holben (2002), Validation of MODIS aerosol optical depth retrieval over land, *Geophys. Res. Lett.*, **29**(12), 8007, doi:10.1029/2001GL013205.
- Chu, D. A., Y. J. Kaufman, G. Zibordi, J. D. Chern, J. Mao, C. Li, and B. N. Holben (2003), Global monitoring of air pollution over land from the Earth Observing System-Terra Moderate Resolution Imaging Spectroradiometer (MODIS), *J. Geophys. Res.*, **108**(D21), 4661, doi:10.1029/2002JD003179.
- Clarke, A. D. (1991), A thermo-optic technique for in situ analysis of size-resolved aerosol physicochemistry, *Atmos. Environ., Part A*, **25**, 635–644.
- Clarke, A. D., et al. (2002), INDOEX aerosol: A comparison and summary of chemical, microphysical, and optical properties observed from land, ship, and aircraft, *J. Geophys. Res.*, **107**(D19), 8033, doi:10.1029/2001JD000572.
- Clarke, A., et al. (2007), Biomass burning and pollution aerosol over North America: Organic components and their influence on spectral optical properties and humidification response, *J. Geophys. Res.*, doi:10.1029/2006JD007777, in press.
- Dubovik, O., and M. D. King (2000), A flexible inversion algorithm for retrieval of aerosol optical properties from Sun and sky radiance measurements, *J. Geophys. Res.*, **105**(D16), 20,673–20,696.
- Fuelberg, H. E., M. J. Porter, C. M. Kiley, J. J. Halland, and D. Morse (2007), Meteorological conditions and anomalies during the Intercontinental Chemical Transport Experiment-North America, *J. Geophys. Res.*, **112**, D12S06, doi:10.1029/2006JD007734.
- Gassó, S., and D. A. Hegg (2003), On the retrieval of columnar aerosol mass and CCN concentration by MODIS, *J. Geophys. Res.*, **108**(D1), 4010, doi:10.1029/2002JD002382.
- Hand, J. L., and S. M. Kreidenweis (2002), A new method for retrieving particle refractive index and effective density from aerosol size distribution data, *Aerosol Sci. Technol.*, **36**, 1012–1026.
- Heintzenberg, J., and R. J. Charlson (1996), Design and applications of the integrating nephelometer: A review, *J. Atmos. Oceanic Technol.*, **13**, 987–1000.
- Holben, B. N., et al. (1998), AERONET—A federated instrument network and data archive for aerosol characterization, *Remote Sens. Environ.*, **66**(1), 1–16.
- Howell, S. G., A. D. Clarke, Y. Shinozuka, V. Kapustin, C. S. McNaughton, B. J. Huebert, S. J. Doherty, and T. L. Anderson (2006), Influence of relative humidity upon pollution and dust during ACE-Asia: Size distributions and implications for optical properties, *J. Geophys. Res.*, **111**, D06205, doi:10.1029/2004JD005759.
- Ichoku, C., L. A. Remer, Y. J. Kaufman, R. Levy, D. A. Chu, D. Tanré, and B. N. Holben (2003), MODIS observation of aerosols and estimation of aerosol radiative forcing over southern Africa during SAFARI 2000, *J. Geophys. Res.*, **108**(D13), 8499, doi:10.1029/2002JD002366.
- Kahn, R., P. Banerjee, D. McDonald, and D. J. Diner (1998), Sensitivity of multiangle imaging to aerosol optical depth and to pure-particle size distribution and composition over ocean, *J. Geophys. Res.*, **103**(D24), 32,195–32,213.
- Kaufman, Y. J., D. Tanre, L. A. Remer, E. F. Vermote, A. Chu, and B. N. Holben (1997), Operational remote sensing of tropospheric aerosol over land from EOS moderate resolution imaging spectroradiometer, *J. Geophys. Res.*, **102**(D14), 17,051–17,067.
- Liu, Y., R. J. Park, D. J. Jacob, Q. Li, V. Kilaru, and J. A. Sarnat (2004), Mapping annual mean ground-level PM<sub>2.5</sub> concentrations using Multiangle Imaging Spectroradiometer aerosol optical thickness over the contiguous United States, *J. Geophys. Res.*, **109**, D22206, doi:10.1029/2004JD005025.
- Liu, Y., J. A. Sarnat, A. Kilaru, D. J. Jacob, and P. Koutrakis (2005), Estimating ground-level PM<sub>2.5</sub> in the eastern united states using satellite remote sensing, *Environ. Sci. Technol.*, **39**(9), 3269–3278.
- Malm, W. C., J. F. Sisler, D. Huffman, R. A. Eldred, and T. A. Cahill (1994), Spatial and seasonal trends in particle concentration and optical extinction in the United States, *J. Geophys. Res.*, **99**(D1), 1347–1370.
- McMurry, P. H., X. Wang, K. Park, and K. Ehara (2002), The relationship between mass and mobility for atmospheric particles: A new technique for measuring particle density, *Aerosol Sci. Technol.*, **36**, 227–238.
- McNaughton, C. S., et al. (2007), Results from the DC-8 inlet characterization experiment (DICE): Airborne versus surface sampling of mineral dust and sea salt aerosols, *Aerosol Sci. Technol.*, **41**, 136–159.
- Nessler, R., E. Weingartner, and U. Baltensperger (2005), Effect of humidity on aerosol light absorption and its implications for extinction and the single scattering albedo illustrated for a site in the lower free troposphere, *J. Aerosol Sci.*, **36**(8), 958–972.
- Pinnick, R. G., J. D. Pendleton, and G. Videen (2000), Response characteristics of the particle measuring systems active scattering aerosol spectrometer probes, *Aerosol Sci. Technol.*, **33**, 334–352.
- Quinn, P. K., and T. S. Bates (2005), Regional aerosol properties: Comparisons of boundary layer measurements from ACE 1, ACE 2, Aerosols99, INDOEX, ACE Asia, TARFOX, and NEAQS, *J. Geophys. Res.*, **110**, D14202, doi:10.1029/2004JD004755.
- Quinn, P. K., D. J. Coffman, T. S. Bates, T. L. Miller, J. E. Johnson, E. J. Welton, C. Neusüss, M. Miller, and P. J. Sheridan (2002), Aerosol optical properties during INDOEX 1999: Means, variability, and controlling factors, *J. Geophys. Res.*, **107**(D19), 8020, doi:10.1029/2000JD000037.
- Quinn, P. K., et al. (2005), Impact of particulate organic matter on the relative humidity dependence of light scattering: A simplified parameterization, *Geophys. Res. Lett.*, **32**, L22809, doi:10.1029/2005GL024322.
- Redemann, J., S. J. Masonis, B. Schmid, T. L. Anderson, P. B. Russell, J. M. Livingston, O. Dubovik, and A. D. Clarke (2003), Clear-column closure studies of aerosols and water vapor aboard the NCAR C-130 during ACE-Asia, 2001, *J. Geophys. Res.*, **108**(D23), 8655, doi:10.1029/2003JD003442.
- Remer, L. A., et al. (2002), Validation of MODIS aerosol retrieval over ocean, *Geophys. Res. Lett.*, **29**(12), 8008, doi:10.1029/2001GL013204.
- Remer, L. A., et al. (2005), The MODIS aerosol algorithm, products, and validation, *J. Atmos. Sci.*, **62**(4), 947–973.
- Russell, P. B., et al. (2007), Multi-grid-cell validation of satellite aerosol property retrievals in INTEx/ITCT/ICARTT 2004, *J. Geophys. Res.*, **112**, D12S09, doi:10.1029/2006JD007606.

- Shinozuka, Y., A. D. Clarke, S. G. Howell, V. N. Kapustin, and B. J. Huebert (2004), Sea-salt vertical profiles over the Southern and tropical Pacific oceans: Microphysics, optical properties, spatial variability, and variations with wind speed, *J. Geophys. Res.*, *109*, D24201, doi:10.1029/2004JD004975.
- Singh, H. B., W. H. Brune, J. H. Crawford, D. J. Jacob, and P. B. Russell (2006), Overview of the summer 2004 Intercontinental Chemical Transport Experiment-North America (INTEX-A), *J. Geophys. Res.*, *111*, D24S01, doi:10.1029/2006JD007905.
- Tang, I. N., and H. R. Munkelwitz (1991), Simultaneous determination of refractive index and density of evaporating aqueous solution droplet, *Aerosol Sci. Technol.*, *15*, 201–207.
- Tanre, D., Y. J. Kaufman, M. Herman, and S. Mattoo (1997), Remote sensing of aerosol properties over oceans using the MODIS/EOS spectral radiances, *J. Geophys. Res.*, *102*(D14), 16,971–16,988.
- Virkkula, A., N. C. Ahlquist, D. S. Covert, W. P. Arnott, P. J. Sheridan, P. K. Quinn, and D. J. Coffman (2005), Modification, calibration and a field test of an instrument for measuring light absorption by particles, *Aerosol Sci. Technol.*, *39*(1), 68–83.
- Wang, J., and S. A. Christopher (2003), Intercomparison between satellite-derived aerosol optical thickness and PM<sub>2.5</sub> mass: Implications for air quality studies, *Geophys. Res. Lett.*, *30*(21), 2095, doi:10.1029/2003GL018174.
- B. E. Anderson, Atmospheric Sciences Division, NASA Langley Research Center, Mail Stop 483, Hampton, VA 23681, USA.
- A. D. Clarke, S. G. Howell, V. N. Kapustin, C. S. McNaughton, Y. Shinozuka, and J. Zhou, School of Ocean and Earth Science and Technology, University of Hawaii, Honolulu, HI 96822, USA. (yohei@hawaii.edu)